**Astronomy
&
Astrophysics**

Abundance analysis of targets for the COROT/MONS asteroseismology missions

II. Abundance analysis of the COROT main targets[*]

H. Bruntt[1], I. F. Bikmaev[2], C. Catala[3], E. Solano[4], M. Gillon[5], P. Magain[5], C. Van't Veer-Menneret[6],
C. Stütz[7], W. W. Weiss[7], D. Ballereau[6], J. C. Bouret[8], S. Charpinet[9], T. Hua[8],
D. Katz[6], F. Lignières[9], and T. Lueftinger[7]

[1] Department of Physics and Astronomy, Aarhus University, Bygn. 520, 8000 Aarhus C, Denmark
   e-mail: bruntt@phys.au.dk
[2] Department of Astronomy, Kazan State University, Kremlevskaya 18, 420008 Kazan, Russia
[3] Observatoire de Paris, LESIA, France
[4] Laboratorio de Astrofísica Espacial y Física Fundamental, PO Box 50727, 28080 Madrid, Spain
[5] Institut d'Astrophysique et de Géophysique, Université de Liège, Allée du 6 Août, 17, 4000 Liège, Belgium
[6] Observatoire de Paris, GEPI, France
[7] Institut für Astronomie, Universität Wien, Türkenschanzstrasse 17, 1180 Wien, Austria
[8] Laboratoire d'Astrophysique de Marseille, France
[9] Laboratoire d'Astrophysique de l'OMP, CNRS UMR 5572, Observatoire Midi-Pyrénées, 14, avenue Edouard Belin,
   31400 Toulouse, France

Abstract. One of the goals of the ground-based support program for the COROT and MONS/RØMER satellite missions is to characterize suitable target stars for the part of the missions dedicated to asteroseismology. We present the detailed abundance analysis of nine of the potential COROT main targets using the semi-automatic software VWA. For two additional COROT targets we could not perform the analysis due to the high rotational velocity of these stars. For five stars with low rotational velocity we have also performed abundance analysis by a classical equivalent width method in order to test the reliability of the VWA software. The agreement between the different methods is good. We find that it is necessary to measure abundances extracted from each line relative to the abundances found from a spectrum of the Sun in order to remove systematic errors. We have constrained the global atmospheric parameters $T_{\rm eff}$, $\log g$, and [Fe/H] to within $70-100$ K, $0.1-0.2$ dex, and 0.1 dex for five stars which are slow rotators ($v \sin i < 15$ km s^{-1}). For most of the stars we find good agreement with the parameters found from line depth ratios, Hα lines, Strömgren indices, previous spectroscopic studies, and also $\log g$ determined from the HIPPARCOS parallaxes. For the fast rotators ($v \sin i > 60$ km s^{-1}) it is not possible to constrain the atmospheric parameters.

Key words. stars: abundances – stars: fundamental parameters

1. Introduction

COROT (COnvection, ROtation, and planetary Transits) is a small space mission, dedicated to asteroseismology and the search for exo-planets (Baglin et al. 2001). Among the targets of the asteroseismology part of the mission, a few bright stars will be monitored continuously over a period of 150 days. These bright targets will be chosen from a list of a dozen F & G-type stars, located in the continuous viewing zone of the instrument. The final choice of targets needs to be made early in the project, as it will impact on some technical aspects of the mission. A precise and reliable knowledge of the candidate targets is required, in order to optimize this final choice.

Among the information which needs to be gathered on the candidate targets, fundamental parameters like effective temperature, surface gravity, and metallicity will play a major role in the selection of targets for COROT. Projected rotation velocities, as well as detailed abundances of the main chemical elements will also be taken into account in the selection process. Thus, the aim of this study is to obtain improved values for the fundamental parameters and abundances of individual elements for the COROT main targets.

This information on the targets will subsequently be used for the selected stars, in conjunction with asteroseismological data obtained by COROT, to provide additional constraints for the modelling of the interior and the atmospheres of these stars.

In Sect. 2 we summarize the spectroscopic observations and data reduction, in Sect. 3 we discuss the determination

---

[*] Based on observations obtained with the 193 cm telescope at Observatoire de Haute Provence, France.

Table 1. Log of the observations for the spectra of the proposed COROT targets we have analysed. The signal-to-noise ratio in the last column is calculated around 6500 Å in bins of 3 km s^{-1}.

HD	Date	UT start	$t_{\exp}$	S/N
43318	19-Jan.-98	22:38	900	120
43587	14-Jan.-98	22:32	1800	250
45067	15-Jan.-98	22:20	1200	260
49434	17-Jan.-98	22:33	600	160
49933	21-Jan.-98	22:17	1200	210
55057	15-Jan.-98	23:10	900	270
57006	10-Dec.-00	00:41	1800	250
171834	05-Sep.-98	19:00	1800	300
184663	18-Jun.-00	01:30	1000	170
46304	17-Jan.-98	22:05	600	170
174866	04-Jul.-01	00:39	1500	190

Table 2. Strömgren photometric indices of the COROT main targets taken from Hauck & Mermilliod (1998). HD 46304 and HD 174866 are shown separately: abundance analysis has not been made for these two stars due to their high $v \sin i$.

HD	V	$b-y$	m_1	c_1	H$_\beta$
43318	5.65	0.322	0.154	0.446	2.644
43587	5.70	0.384	0.187	0.349	2.601
45067	5.87	0.361	0.168	0.396	2.611
49434	5.74	0.178	0.178	0.717	2.755
49933	5.76	0.270	0.127	0.460	2.662
55057	5.45	0.185	0.184	0.876	2.757
57006	5.91	0.340	0.168	0.472	2.625
171384	5.45	0.254	0.145	0.560	2.682
184663	6.37	0.275	0.149	0.476	2.665
46304	5.60	0.158	0.175	0.816	2.767
174866	6.33	0.122	0.178	0.960	2.822

of the fundamental parameters from spectroscopy, photometry and HIPPARCOS parallaxes and we summarize previous spectroscopic studies of the target stars. In Sect. 4 we describe the three different methods we have used for abundance analysis. In Sect. 5 we discuss how we constrain the fundamental atmospheric parameters using abundance results for a grid of models. In Sect. 6 we discuss the abundances we have determined. Lastly, we give our conclusions in Sect. 7.

2. Spectroscopic observations

We have obtained spectra of each one of the 11 candidate main targets of COROT, using the ELODIE spectrograph attached to the 1.93 m telescope at Observatoire de Haute-Provence (OHP). ELODIE is a fiber-fed cross-dispersed Echelle spectrograph, providing a complete spectral coverage of the 3800–6800 Å region, at a resolution of $R = 45\,000$ (Baranne et al. 1996). Table 1 gives the log of the observations for the spectra used in this analysis.

2.1. Data reduction

We used the on-line INTER-TACOS reduction package available at OHP (Baranne et al. 1996). This software performs bias and background light subtraction, spectral order localization, and finally extracts spectral orders using the optimal extraction procedure (Horne 1986). The high spatial frequency instrumental response is corrected by dividing the stellar spectra by the spectrum of a flat-field lamp. Wavelength calibration is provided by spectra of a Th/Ar lamp, using a two-dimensional Chebychev polynomial fitting to the centroid locations of the Th/Ar lines.

Special care was taken to correct for the grating blaze function, as differences in the spectrograph illumination between stellar and flat-field light beams usually result in an imperfect correction. Instead of using a flat-field spectrum, we have therefore used a high signal-to-noise spectrum of an O-type star, 10 Lac, to determine the blaze function. The orders of the 10 Lac spectrum were examined one by one, and the line-free regions of each order were identified. The blaze function at each spectrograph order was then represented by cubic splines fitted to these line-free regions, and the stellar spectra were

subsequently divided by this newly determined blaze function. This procedure results in an adequate blaze correction, producing in particular a good match of adjacent orders in the overlapping regions. Note also that ELODIE is a very stable instrument, so that only one spectrum of 10 Lac was used to define the blaze function, although the observations reported here span several years.

Since the overall blaze function was removed by a star of much earlier spectral class than the observed F and G-type stars the continuum level was not entirely flat. Hence we made cubic spline fits to make the final continuum estimate. For the overlapping part of the orders we made sure that the overlap was better than 0.5%.

We are aware of the problem of fitting low-order splines to correct the continuum. In this process we manually mark the points in the spectrum which we assume are at the continuum level. When using the VWA software (Bruntt et al. 2002, cf. Sect. 4.2) we can inspect the fitted lines and in this way detect problems with the continuum level. In these cases we reject the abundances found for these lines (cf. Sect. 4.5). Alternatively, one could select "continuum windows" from a synthetic spectrum or a spectrum of the Sun and use this to correct the continuum level. This has been attempted for one of our program stars in Sect. 4.4.

3. Fundamental atmospheric parameters

In this section we will discuss previous results for the fundamental atmospheric parameters of the proposed COROT targets. We will present the results from the calibration of Strömgren photometry, line depth ratios, Hα line wings, and HIPPARCOS parallaxes.

3.1. Strömgren photometry

The Strömgren indices of the target stars are taken from the catalogue of Hauck & Mermilliod (1998) and are listed in Table 2. We have used the software TEMPLOGG (Rogers 1995; see also Kupka & Bruntt 2001) to find the appropriate calibration to obtain the basic parameters, i.e. $T_{\rm eff}$, $\log g$, and [M/H]$_{\rm phot}$. These

Table 3. Overview of the parameters of the proposed COROT main targets. The first column is the HD number and column 2 is $T_{\rm eff}$ determined from line depth ratios with formal errors in parenthesis (Kovtyukh et al. 2003). Column 3 gives the temperatures found from the Hα wings (the internal error is 50 K). Columns 4–6 are the atmospheric parameters derived from Strömgren photometry when using the TEMPLOGG software (typical errors are 200 K, 0.3 dex, and 0.2 dex). Columns 7 and 8 are the masses found from evolution tracks (cf. Fig. 1) and $\log g_\pi$ values found from the HIPPARCOS parallaxes; the numbers in parenthesis are the estimated standard errors. In Col. 9 we list $v \sin i$ where the typical error is 5–10%.

HD	Line depth ratio $T_{\rm eff}$ [K]	Hα wings $T_{\rm eff}$ [K]	Strömgren indices $T_{\rm eff}$ [K]	$\log g$	[M/H]$_{\rm phot}$	Evolution tracks & parallax $M/M_\odot$	$\log g_\pi$	Spectral synthesis $v \sin i$ [km s^{-1}]
Sun	5770(5)	–	5778[a]	4.44[a]	+0.00[a]	1[a]	4.44[a]	2[b]
43318	6191(17)	6100	6400	4.19	−0.15	1.23(17)	3.96(14)	8
43587	5923(8)	5850	5931	4.31	−0.11	1.02(20)	4.29(15)	2.5[b]
45067	6067(6)	5900	6038	4.03	−0.22	1.08(17)	3.96(15)	<7[b]
49434	–	6950	7304	4.14	−0.01	1.55(14)	4.25(11)	84
49933	–	6400	6576	4.30	−0.45	1.17(18)	4.20(14)	14
55057	–	6750	7274	3.61	+0.10	2.12(22)	3.66(12)	120
57006	6181(7)	6000	6158	3.72	−0.13	1.28(17)	3.58(16)	9
171834	–	6550	6716	4.03	−0.22	1.40(17)	4.13(13)	63
184663	–	6450	6597	4.25	−0.17	1.29(14)	4.19(15)	53
46304	–	7050	7379	3.93	−0.09	1.68(14)	4.18(11)	200
174866	–	7200	7865	3.86	−0.18	1.77(14)	3.86(15)	165

[a] The fundamental parameters for the Sun are also given in the table, although we have not determined its parameters; the exception is our estimate of $T_{\rm eff}$ from line depth ratios.
[b] With the resolution of the ELODIE spectrograph ($R = 45\,000$) it is not possible to measure $v \sin i$ below 7 km s^{-1} directly.

parameters are given in Table 3. The accuracy of the parameters $T_{\rm eff}$, $\log g$, and [M/H]$_{\rm phot}$ are around 200–250 K, 0.3 dex, and 0.2 dex according to Rogers (1995).

A catalogue of Strömgren indices determined for all primary and secondary targets for COROT is available from the GAUDI database[1]. We also used these data to get the fundamental parameters. For most stars both $T_{\rm eff}$ and $\log g$ agree within the uncertainties quoted above. But for HD 43587 and HD 45067 we find a large discrepancy, i.e. $\log g$ higher by 0.2/0.3 dex and a higher $T_{\rm eff}$ by 350/300 K for the two stars, respectively. This is a clear indication that it is worthwhile to use several methods to try to determine the fundamental parameters.

3.2. Temperature calibration from line depth ratios

Kovtyukh et al. (2003) have used spectra of 181 main sequence F-K type stars to calibrate the dependence of line depth ratios on $T_{\rm eff}$. They used observed spectra from ELODIE (the same spectrograph we used) and their sample of stars consisted of stars for which $T_{\rm eff}$ is well determined, e.g. using the infrared flux method.

We measured line depths by fitting a Gaussian profile to each line, i.e. the depth of the Gaussian defines the line depth. We used $T_{\rm eff}$ from the Strömgren photometry as our initial guess (assuming the error is $\sigma(T_{\rm eff}) = 250$ K) to select which of the calibrations by Kovtyukh et al. (2003) that were valid. We note that for each pair of lines defining the ratio calibration the species of elements are typically different (e.g. Si/Ti, Fe/S etc.), but we refer to Kovtyukh et al. (2003) for details.

Typically 50–80 line depth ratios between lines could be used. We then calculated the mean $T_{\rm eff}$ and rejected 3σ outliers and recalculated $T_{\rm eff}$. The calibrations are only valid in the range 4000–6150 K so only the four coolest COROT target stars could be used with this method.

The results are given in Table 3 for these stars and the Sun. The $T_{\rm eff}$ we determine from the spectrum of the Sun agrees with the canonical value of $T_{\rm eff} = 5777$ K. The quoted errors of 5–17 K on the temperatures are formal errors, and systematic errors of the order 50–100 K must be added.

3.3. Temperatures from Hα lines

We have estimated $T_{\rm eff}$ of the stars considered in this study using their Hα line profiles, following a method proposed by Cayrel et al. (1985) and Cayrel de Strobel et al. (1994). The method is based on the property of Hα that it is insensitive to any atmospheric parameter except $T_{\rm eff}$ in in the range between 5000–8500 K.

In order to overcome problems due to continuum placement, we compute the ratio of the observed Hα profile to that of the Sun, observed with the same instrumental configuration (spectrum of the solar reflected light on the moon surface), then compare it to the corresponding ratio of theoretical profiles computed from a grid of models. The best fit between computed and observed profile ratios gives the effective temperature with an internal error bar of about ±50 K.

We have used the new grids of ATLAS9 models presented in Heiter et al. (2002), choosing the models with MLT convection treatment for $T_{\rm eff}$ lower than 8750 K, with the low value for

---

[1] http://sdc.laeff.esa.es/gaudi/

the efficiency parameter of the convection, following Fuhrmann et al. (1993), Axer et al. (1994), and Heiter et al. (2002).

The H α line profile is computed using BALMER9 (Kurucz 1998) which includes the Vidal et al. (1973) unified theory for the Stark Broadening and also takes into account the self resonance mechanism in the computation of the H α profile.

This method if found to be reliable for $T_{\rm eff}$ between 5500 and 8500 K. Below 5500 K, the H α profile is not sensitive enough to $T_{\rm eff}$, and does not constitute a good temperature tracer. Above 8500 K, the H α wings depend only slightly on $T_{\rm eff}$, and start to become sensitive to gravity.

We find that the final $T_{\rm eff}$ estimate is insensitive to the choice of convection description. On the other hand Heiter et al. (2002) find that the $(b - y)$ index and hence $T_{\rm eff}$ found from the Strömgren indices is sensitive to the convection description.

The $T_{\rm eff}$ measurements with this method are also reasonably insensitive to rotation, for $v \sin i$ below 80–100 km s^{-1}.

3.4. Comparison of temperature estimators

Except for HD 43318 there is very good agreement between $T_{\rm eff}$ from the Strömgren calibration (TEMPLOGG) and the line depth ratios. However, $T_{\rm eff}$ of HD 43318 is on the border of the valid range of the latter calibration. The $T_{\rm eff}$ from the H α lines agrees with the other two methods but only for stars with low $v \sin i$. The stars in our sample with moderate $v \sin i$ also have the highest $T_{\rm eff}$, and the discrepant results for the H α lines may be an indication that this method cannot be used for these stars.

3.5. Using HIPPARCOS parallaxes to determine log g

We have used HIPPARCOS parallaxes (ESA 1997) to find the surface gravities of the stars. We use the equation $\log g_\pi = 4[T_{\rm eff}] + [M] + 2\log \pi + 0.4(V + BC_V + 0.26) + 4.44$, where $[T_{\rm eff}] = \log(T_{\rm eff}/T_{\rm eff \odot})$ and $[M] = \log(M/M_\odot)$. We use $T_{\rm eff}$ from TEMPLOGG and we determine the bolometric correction BC_V from Bessell et al. (1998): we used their results for solar metallicity and no overshoot. We have estimated the masses of the stars by using the evolution tracks by Girardi et al. (2000). The evolution tracks for solar metallicity are shown in Fig. 1 in which the locations of the COROT targets are also shown along with error bars. We have made interpolations in models for metallicity $Z = 0.019$ (solar) and $Z = 0.008$. For example, HD 49933 has the lowest metallicity in the sample: the derived mass is $M/M_\odot = 1.17$, significantly lower than estimated from its position relative to the solar metallicity isochrones shown in Fig. 1.

The determination of $\log g$ when using the calibration of Strömgren indices and the HIPPARCOS parallax are shown in Fig. 2. Mean error bars which are representative for all the stars are shown in the lower right corner. Note that the two most important error sources for $\log g_\pi$ are $T_{\rm eff}$ and the mass. The results for $\log g_\pi$ and $\log g_{\rm phot}$ agree very well. The mean difference is $(\log g_{\rm phot} - \log g_\pi) = 0.05 \pm 0.22$.
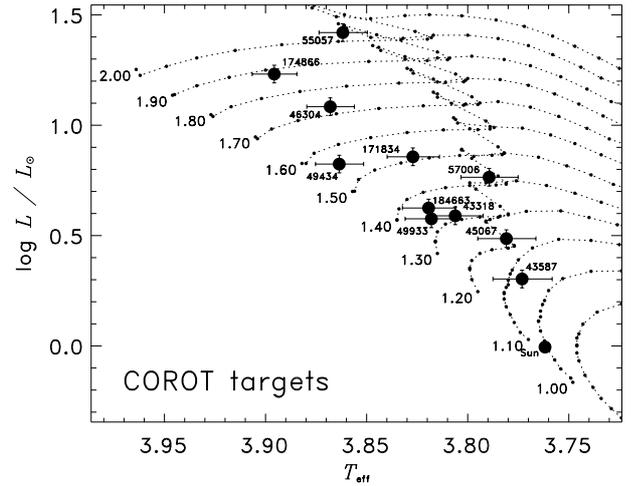
Fig. 1. Evolution tracks from Girardi et al. (2000) for solar metallicity. The positions of the proposed COROT targets and the Sun are shown.
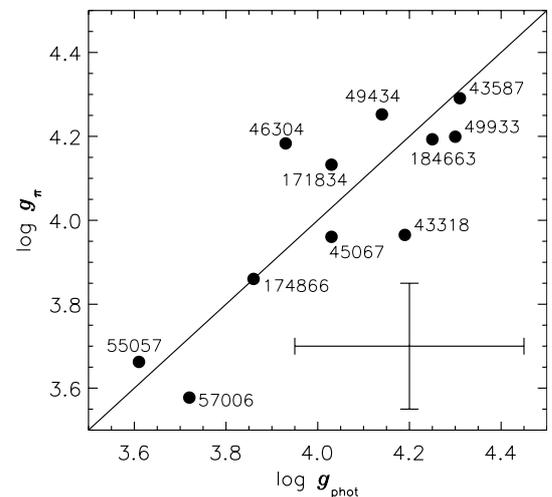
Fig. 2. Comparison of the $\log g_\pi$ values found from the HIPPARCOS parallaxes and $\log g_{\rm phot}$ from TEMPLOGG using Strömgren indices. The straight line is added to aid the eye. Typical error bars are shown.

3.6. Previous spectroscopic studies

Lastennet et al. (2001) (hereafter LLB) have analyzed some of the potential COROT targets and they used the same spectra we have used in this study: we have six stars in common with LLB (compared in Table 4). LLB have also used the H α hydrogen lines to determine $T_{\rm eff}$. The fact that the H α line covers three Echelle orders makes the determination of the continuum a difficult task, hence the error on $T_{\rm eff}$ is around 250 K. LLB have compared Johnson and Strömgren photometric indices of observations and calculated model atmospheres in order to determine $T_{\rm eff}$, $\log g$, and [Fe/H]. The $T_{\rm eff}$ estimates made by LLB agree well with the results from TEMPLOGG although the two different techniques (H α lines and photometry) show systematic differences at the 100 K level. LLB have used Fe I and Fe II lines in a limited spectral region to estimate [Fe/H] and $\log g$ to within 0.2 dex and 0.5 dex and these results also agree with TEMPLOGG within the error bars. The exception is

Table 4. Results of various efforts to determine the parameters of the COROT targets. The results of this study are given as references 1a–c (corresponding to method A–C as described in Sect. 4). The references are given in Table 5.

HD	$T_{\rm eff}$	$\log g$	[Fe/H]	Ref.
43318	6190(90)	3.70(0.15)	−0.21(11)	1a
–	6347	4.07	−0.17	4
–	6257	4.09	−0.19	7
–	6320(100)	4.5(0.2)	+0.0(0.15)	9a
–	6250(250)	4.0(0.5)	−0.3(0.2)	9b
43587	5870(60)	4.20(0.15)	−0.09(0.11)	1a
–	5780(100)	4.25(0.15)	−0.05(0.11	1b
–	5867(20)	4.29(0.06)	−0.05(0.08)	1c
–	5775		−0.08(0.04)	5
–	5931(100)		−0.00(0.05)	6
–	5720(100)	4.3(0.4)	−0.2(0.10)	9a
–	6000(250)	4.5(0.5)	−0.1(0.2)	9b
–	5795		−0.03	11
–			−0.03	12
45067	5970(100)	3.80(0.15)	−0.17(0.11)	1a
–	6050(100)	4.00(0.15)	−0.04(0.11)	1b
–	6056	4.17	−0.16	2
–	5940(100)	3.8(0.35)	−0.1(0.08)	9a
–	6000(250)	4.0(0.5)	−0.1(0.2)	9b
49434	7300(200)	4.4(0.4)	−0.04(0.21)	1a
–			−0.13(14)	3
–	7240(150)	4.0(0.25)	−0.1(0.25)	9a
–	7250(250)			9b
49933	6780(70)	4.3(0.2)	−0.30(0.11)	1a
–	6472	4.17	−0.35	2
–	6595	4.16	−0.43	4
–	6300	4.5	−0.88	8
–	6600(150)	4.3(0.25)	−0.6(0.15)	9a
–	6500(250)	4.0(0.5)	−0.5(0.2)	9b
–	6545	4.00	−0.35	10
55057	7580(250)	3.6(0.5)	+0.14(0.21)	1a
57006	6180(70)	3.60(0.15)	−0.08(0.11)	1a
–	6100(100)	3.50(0.15)	−0.04(0.11)	1b
171834	6840(200)	4.6(0.5)	−0.25(0.21)	1a
–	6670	4.05	−0.42	2
–	6700(150)	3.9(0.25)	−0.5(0.15)	9a
–	6750(250)			9b
184663	6600(200)	4.5(0.5)	−0.19(0.21)	1a
–	6535	4.22	+0.03	2

for their star HD 46304 but this is probably due to its high $v \sin i = 200$ km s^{-1}.

Vogt et al. (2002) have found a low-mass companion around HD 43587 in a campaign to search for exoplanets. From their Keck spectra they find $T_{\rm eff} = 5795$ K, [Fe/H] = −0.03, and $v \sin i = 2.7$ km s^{-1} (Vogt et al. 2002, have not quoted errors on $T_{\rm eff}$ and metallicity). D. Fisher (private communication) has re-analysed the Keck spectrum and finds $T_{\rm eff} = 5931 \pm 100$ and [Fe/H] = 0.00 ± 0.05.

The extensive catalogue by Cayrel de Strobel et al. (2001) contains fundamental atmospheric parameters found in the literature based on analyses of medium-high resolution spectra. The catalogue contains results from several studies for most of the stars examined here, but unfortunately, no individual error

Table 5. The references for Table 4.

Ref. 1a: Optimal parameters found using method A (VWA).
Ref. 1b: Fixed parameters used for method B.
Ref. 1c: Optimal parameters found using method C.
Ref. 2: Balachandran (1990).
Ref. 3: Bruntt et al. (2002).
Ref. 4: Edvardsson et al. (1993).
Ref. 5: Favata et al. (1997).
Ref. 6: Fisher, D. (private communication).
Ref. 7: Gratton et al. (1996).
Ref. 8: Hartmann & Gehren (1988).
Ref. 9a: Lastennet et al. (2001) (colours).
Ref. 9b: Lastennet et al. (2001) (spectroscopy).
Ref. 10: Perrin (1976).
Ref. 11: Vogt et al. (2002).
Ref. 12: Zakhozhaj & Shaparenko (1996).

estimates are given by the original authors. In Table 4 we summarize the parameters from these studies (Refs. 2, 4, 5, 7 & 8) along with our new results (Refs. 1a–c). The references in column five of Table 4 are listed in detail in Table 5. Note that for LLB we give two results: (9a) which corresponds to their result when comparing observed and synthetic colour-indices in $B - V$, $U - B$, and $b - y$; (9b) $T_{\rm eff}$ is determined from the Hα line while $\log g$ and [Fe/H] are determined from a small sample of Fe I and Fe II lines in a region around 6130 Å.

4. Abundance analysis

Nine stars were analysed with the semi-automatic software VWA (H. Bruntt – HB) while two groups (I. F. Bikmaev – IFB – and M. Gillon/P. Magain – MG/PM) made an independent analysis by means of using the equivalent width of isolated lines for some of the slowly rotating stars. We will describe each method here before comparing the results. Firstly, we shall discuss the atmospheric models we have applied.

4.1. Atmospheric models

For method A and B (see below) we have used a modified version of the ATLAS9 code (Kurucz 1993) for the calculation of the atmospheric models (Kupka 1996; Smalley & Kupka 1997) in which turbulent convection theory in the formulation of Canuto & Mazzitelli (1991, 1992) is implemented. For method C the standard ATLAS9 models (Kurucz 1993) with mixing length parameter $\alpha = 1.25$ were used.

For the extraction of models in a grid with different $T_{\rm eff}$ and $\log g$ we have used interpolation in the grid of models (also modified ATLAS9 models) distributed by Heiter et al. (2002). We have used these interpolated models to make abundance analysis in order to constrain the fundamental parameters in Sect. 5.

4.2. Automatic abundance analysis with VWA (Method A)

We have used the semi-automatic software package VWA (Bruntt et al. 2002) to carry out the abundance analysis of

nine COROT targets. For each star the software selects the least blended lines from atomic line list data extracted from the VALD data base (Kupka et al. 1999). The atomic data consist of the element name and ionization state, wavelength, excitation potential, oscillator strength, and damping parameters. For each selected line the synthetic spectrum is calculated and the input abundance is changed iteratively until the equivalent width of the observed and synthetic line match. We used SYNTH (version 2.5, see Valenti & Piskunov 1996) to calculate the synthetic spectrum. This software was kindly provided by N. Piskunov (private communication).

4.2.1. Rotational velocities

In order to be able to compare the observed and synthetic spectra the latter is convolved by the instrumental profile (approximated by a Gaussian) and a rotational broadening profile. The projected rotational velocities were determined by fitting the synthetic spectrum of a few of the least blended lines to the observed spectrum by convolving with different rotation profiles. Note that we have used zero macroturbulence, and thus our quoted values for $v \sin i$ is a combination of the effects of rotational broadening and macroturbulence. The accuracy of $v \sin i$ by this method is about 5–10%. LLB used a more refined method (see Donati et al. 1997) but our results agree within the estimated errors. The exception is for HD 43587 for which we have found 7 km s^{-1} while Vogt et al. (2002) find $v \sin i = 2.7$ km s^{-1}. Note that D. Fisher finds $v \sin i = 2.2$ km s^{-1} from the same spectrum (private communication). These lower values agrees with LLB and consequently we have used a low value of $v \sin i = 2.5$ km s^{-1}. The reason for the apparent discrepancy is simply the limit of the spectral resolution of the ELODIE spectrograph i.e. $v = c/R \simeq 7$ km s^{-1}. Note that since VWA relies on the measurement of equivalent widths small errors in $v \sin i$ will have a negligible effect on the derived abundances.

4.2.2. Measuring abundances relative to the Sun

During our analyses with VWA we have found that when measuring abundances relative to the same lines observed in the Sun there is a dramatic decrease in the error. Since the abundance of the Sun is well-known (e.g., Grevesse & Sauval 1998) we have decided to make a differential analysis. There are several sources of error that may affect the derived abundances but the most important error is erroneous $\log gf$ values. Incorrect removal of scattered light when reducing the spectra will cause systematic errors.

In Fig. 3 we show the iron abundance for several lines versus both equivalent width and lower excitation potential for HD 57006. In the *top* panel we show the direct results while in the *bottom* panel the abundances are measured relative to the results for the Sun (line-by-line). For the zero point we used $\log N_{\rm Fe}/N_{\rm tot} = -4.54$ from Grevesse & Sauval (1998). The open symbols are used for neutral ion lines (Fe I) and filled symbols for ionized Fe lines (Fe II).
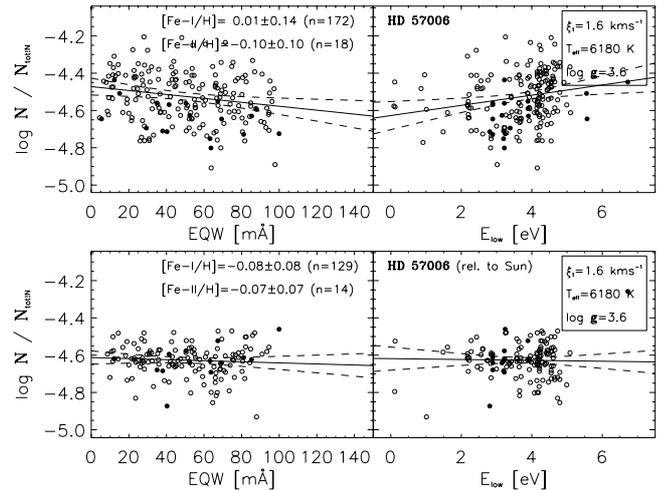
Fig. 3. Iron abundances from lines in the spectrum of HD 57006. Open symbols are neutral iron lines and solid symbols are Fe II lines. The *top* panel shows the raw abundances while in the *bottom* panel the abundances are relative to the abundances (line-by-line) found for the Sun. The abundances are plotted versus equivalent width and excitation potential. The mean abundances and standard deviation are given in each panel and the atmospheric model parameters are found in the boxes. The straight lines are linear fits to the neutral iron lines and the dashed curves indicate the $3\,\sigma$ interval for the fit.

Note the dramatic ~40% decrease in the uncertainty for the neutral ion lines when measuring relative to the Sun (*bottom* panel in Fig. 3). Also, the discrepancy in abundance found from Fe I and Fe II lines is removed. For the applied atmospheric model of HD 57006 there is no correlation with either equivalent width nor excitation potential. Also, both Fe I and Fe II give the same result which indicates that the applied model is correct.

For the results presented in this work we have measured abundances relative to the abundance found for the same lines in the spectrum of the Sun. However, we have not done this for the star HD 49933 and the stars with higher $v \sin i$ since we see no significant improvement for these stars. The reason is that these stars are much hotter than the reference star ($\Delta T_{\rm eff} > 1000$ K). This means that the Sun and the hotter stars have relatively few lines in common which are suitable for abundance analysis. However, it is likely that this is an indication of inadequacies of the model atmospheres.

4.2.3. Adjusting the microturbulence

For each model we adjust the microturbulence ξ_t until we see no correlation between the abundances and equivalent widths found for the Fe I, Cr I, and Ni I lines. To minimize the effect of saturated lines we only use lines with equivalent width below 100 mÅ and for Fe we only use lines with excitation potential in the range 2–5 eV to minimize the effect of erroneous $T_{\rm eff}$ of the model atmosphere. For some stars only Fe could be used due to a lack of non-blended Cr and Ni lines. For the slowly rotating stars ($v \sin i < 25$ km s^{-1}) the error on ξ_t is about 0.1–0.2 km s^{-1}, for the stars rotating moderately fast ($50 < v \sin i < 85$ km s^{-1}) the error is 0.5 km s^{-1}, and 0.7 km s^{-1} for

HD 55057 which has $v \sin i = 120$ km s^{-1}. The contribution to the error on the abundances from the uncertainty of the microturbulence is about 0.03 dex for Fe for the slow rotators while for stars with the highest $v \sin i$ (HD 49434 and HD 55057) the errors in the abundances are of the order 0.07–0.10 dex.

For each star we made the abundance analysis for a grid of models in order to be able to constrain T_{eff} and $\log g$ which will be discussed in Sect. 5.

4.3. "Classical" abundance analysis (Method B)

"Classical" abundance analysis was applied (IFB) to three of the slowly rotating COROT targets – HD 43587, HD 45067, and HD 57006 – and to the solar spectrum (observed reflection from the Moon).

Model atmospheres were calculated as described in Sect. 4.1 with the adopted parameters of T_{eff}, $\log g$, and solar composition. Effective temperatures were determined by using Johnson and Strömgren color-indices extracted from SIMBAD data base and the $\log g$ parameters were determined by using HIPPARCOS parallaxes as outlined in Sect. 3.5. The values we have used are given in Table 4 marked with Ref. 1b. These parameters were not changed during our analysis with method B.

Equivalent widths of all identified unblended and some partially blended spectral lines were measured by using DECH software based on PC (Galazutdinov 1992). Abundance calculations were performed in the LTE approximation by using WIDTH9 (Kurucz 1993; with modifications by V. Tsymbal and L. Mashonkina for PC, private communication). Atomic parameters of the spectral lines were extracted from the VALD data base with corrections of oscillator strengths in a few cases as described in the paper of Bikmaev et al. (2002).

Lines with equivalent widths <100 mÅ were used when possible to decrease influences of microturbulence and inaccurate damping constants. For each star the microturbulence was chosen as to minimize the correlation between the abundances and equivalent widths found for Fe, Cr, Ti, Ni, and Co lines.

4.4. Abundance analysis after continuum re-normalisation (Method C)

A somewhat different approach was followed by two of us (MG and PM) and tested on HD 43587.

First, the continuum was redetermined on the basis of a number of pseudo-continuum windows selected from inspection of the Jungfraujoch solar atlas (Delbouille et al. 1973). These windows were selected to be as close as possible to the true continuum and the mean level was measured in each of them. In all cases, it is between 99% and 100% of the true continuum. The same windows are used for the program star, after correction for its radial velocity and after checking that no telluric lines enter the window because of the Doppler shift. The mean flux is then measured in the stellar windows and a table is constructed, containing the ratio of the mean flux in the star versus the mean flux in the Sun. A spline curve is then fitted through these points and the stellar spectrum is divided by that curve, thus providing our re-normalized spectrum. It may differ

from the normalization described in Sect. 2.1 by ~1%, which is not negligible at all when weak lines are considered.

Then, a list of very good lines is selected by inspection of the solar atlas, and equivalent widths (*EW*s) are measured by least-squares fitting of Gaussian and Voigt profiles. Voigt profiles are generally necessary to adequately fit the lines in the very high resolution solar atlas, as well as for the medium and strong lines in the stellar spectrum. For the weakest stellar lines, Gaussians are generally adequate. The fitted profile is compared to the observed one and the line is rejected if any significant discrepancy appears (e.g. line asymmetries).

Both the star and the Sun are analysed by using models extracted from the same grid (ATLAS9 models; Kurucz 1993). The line oscillator strengths are adjusted so that the solar *EW*s are reproduced, using the adopted solar model and the known solar atmospheric parameters and abundances (similar to what is described in Sect. 4.2.2). Whenever possible, we use damping constants as calculated by Anstee & O'Mara (1995), which have proved to be quite accurate (Anstee et al. 1997; Barklem & O'Mara 2000).

The microturbulence is determined in order to remove any correlation of the computed abundance with the line *EW*, using sets of lines from the same ion and similar excitation potentials. We chose to determine the effective temperature by pure spectroscopic means, using excitation equilibria, i.e. by ensuring that abundances deduced from lines of the same ionic species do not depend on the line excitation potential. The surface gravity was determined from ionization equilibria, by ensuring that lines of neutral and ionic species of the same element give the same abundance.

As an illustration of the coherence of the method, let us consider the determination of the most critical parameter, i.e. T_{eff}. We used three excitation equilibria, which give the following T_{eff}: 5866 ± 18 K (Fe I), 5850 ± 102 K (Cr I) and 5880 ± 57 K (Ni I). The error bars are deduced from the uncertainty in the slope of a straight line fitted to abundances *vs.* excitation potential. A weighted mean gives $T_{\mathrm{eff}} = 5867 \pm 17$ K, taking into account the three individual error bars as well as the scatter in the three determinations. The internal error bar on T_{eff}, taking into account the uncertainties in the other parameters, amounts to 20 K. The other parameters are: $\log g = 4.29 \pm 0.06$ and $v_{\mathrm{turb}} = 2.13 \pm 0.1$ km s^{-1}.

4.5. Comparison of the abundance analysis methods

The three methods described above have different advantages and disadvantages. Most importantly, VWA (method A) relies on the computation of the synthetic spectrum and thus this method can be used for stars with moderately high $v \sin i$ when a mild degree of blending of lines is tolerated. Also, VWA is a semi-automatic program and the user may easily inspect if the fitted lines actually match the observed spectrum. When comparing the observed and synthetic spectrum obvious problems with the continuum level can be found: errors of just 2% of the continuum level will give large differences in the derived abundance – perhaps as much as 0.1–0.2 dex and such lines are rejected after visual inspection.
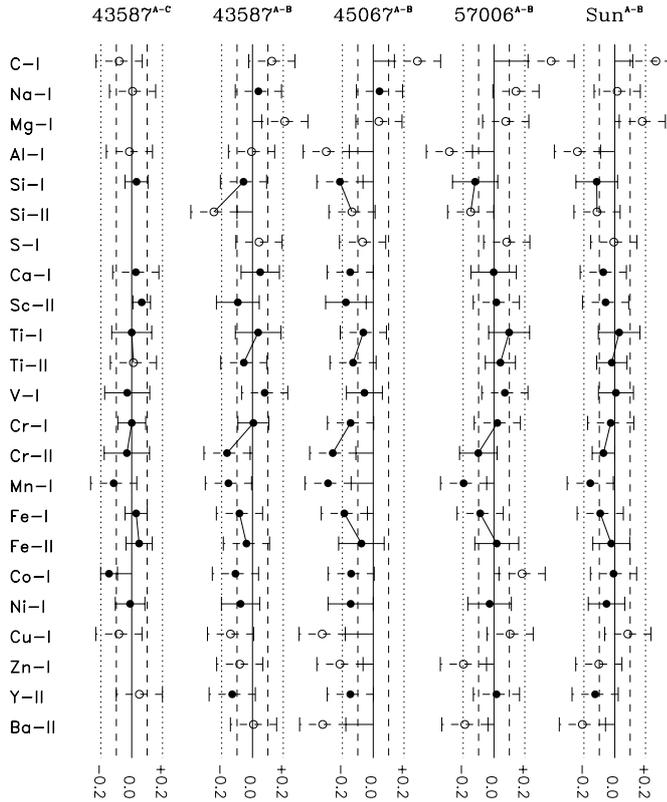
Fig. 4. Comparison of the abundance analysis results for the three different methods. We show the differences in the overall abundances for several elements in the sense method A *minus* method B or C (as indicated above the star name). For HD 43587 we have compared the result from method A (vwa) with both method B and C, while for the remaining stars we only compare method A and B. Open symbols indicate that less than five lines were used. The error bars are the combined standard deviation of the mean for the two methods.

Method B and C both rely on measuring equivalent widths. It is a much faster method computationally, but special care has to be taken to avoid systematic errors from line blends.

In Fig. 4 and in Table 6 we show the comparison of the final abundance analysis results using the three methods described above. We show the differences in abundance in the sense "method A" *minus* "method B". We show results for four different stars with low $v \sin i$ for which both these methods are applicable. For the star HD 43587 we also show result "method A" *minus* "method C". The differences refer to the mean abundances, i.e. the lines are not necessarily the same in the different analyses.

The plotted error bars in Fig. 4 are calculated as the quadratic sum of the standard deviation of the mean for each method. In the cases where we have fewer than five lines we have no good estimate of the error, but from the elements with more lines we find that an overall error of 0.15 dex seems plausible. Thus, in these cases we have plotted a dashed error bar corresponding to 0.15 dex.

The comparison of method A and C for HD 43587 shows excellent agreement for all elements despite the quite different approaches. We emphasize that $T_{\rm eff}$ and $\log g$ have been adjusted as a part of the analysis for these two methods and the

agreement is remarkable, $\Delta T_{\rm eff} = 3 \pm 62$ K, $\Delta \log g = -0.09 \pm 0.16$, Δ[Fe/H]$ = -0.04 \pm 0.14$; see Table 4 for the individual parameters (Refs. 1a and 1c). However, the results from method C have significantly lower formal error on the fundamental parameters. It is likely that the renormalization of the spectrum done with method C is the reason for this improvement, and should be considered in future analyses. The good agreement in the derived fundamental parameters may be an indication that the errors quoted in Table 4 for method A (Ref. 1a) are too large.

In this context we mention Edvardsson et al. (1993) who carried out an abundance study of 189 slowly rotating F and G type stars using data of similar quality. Edvardsson et al. (1993) used fixed values for the atmospheric parameters and found abundances from a small number of lines. Their quoted rms scatter on the abundances is lower than we find here, but this is may be due to the small number of carefully selected lines. For example Edvardsson et al. (1993) use typically ~15 Fe I lines while in this study we use ~150−200 Fe I lines. More importantly, Edvardsson et al. (1993) normalized their spectra by defining "continuum windows" from spectra of the Sun and Procyon. The fact that Edvardsson et al. (1993) obtain abundances with smaller scatter may indeed be due to their careful normalization of the spectra.

The comparison between method A and B show significant systematic differences of the order 0.05−0.10 dex between neutral and ionized abundances of Ti, Cr, and Fe. The worst case is for star HD 45067 where we find a systematic offset of 0.1 dex between method A and B. The reason for these discrepancies is that the models used by vwa and the classical analysis have slightly different parameters, i.e. differences in $\log g$ and $T_{\rm eff}$ of the order 0.1−0.2 dex and 80−100 K.

Based on the generally good agreement between the three analyses, we have used the results from method A (vwa) for all the stars since they were analysed in a homogeneous way. In Sects. 5 and 6 we will describe in detail the analysis of the results from vwa.

5. Constraining model parameters

In order to measure the sensitivity of the derived abundances on the model parameters we have made the abundance analysis for a grid of models for each star. For this purpose we used the vwa software. For the initial model we have used $\log g$ values from HIPPARCOS parallaxes and metallicity from TEMPLOGG. For $T_{\rm eff}$ we used results from TEMPLOGG for the hot stars but we used the result from line depth ratios for the cooler stars (as discussed in Sect. 3). We have then carried out abundance analysis of models with lower and higher values of $T_{\rm eff}$ and $\log g$, i.e. at least five models for each star. For each model we adjust the microturbulence to minimize the correlation between abundance of Fe I, Cr I, and Ti I lines and the measured equivalent width.

Changes in the model temperature will affect the depth of neutral lines while changes in $\log g$ will mostly affect the lines of the ionized elements. Furthermore, changes in $T_{\rm eff}$ will affect the correlation of Fe abundances (and in some cases Cr and Ni) and the lower excitation potential ($E_{\rm low}$;

Table 6. Comparison of the abundances of the main elements found by three different methods. For each star and element we give the difference in abundance ΔA in the sense method A *minus* method B or C. The numbers in parenthesis are the combined rms standard deviations, but only given if at least five lines are used for both methods. For example, $\Delta A = -0.03(14)$ for V I in Col. HD 43587[A-C] means the difference in abundance found with method A and C is -0.03 ± 0.14. The number n is the number of lines used for each method. This data is plotted in Fig. 4.

	HD 43587[A-C]		HD 43587[A-B]		HD 45067[A-B]		HD 57006[A-B]		Sun[A-B]	
	ΔA	n_A/n_C	ΔA	n_A/n_B	ΔA	n_A/n_B	ΔA	n_A/n_B	ΔA	n_A/n_B
C I	−0.08	3/2	+0.13	3/2	+0.29	3/3	+0.37	3/2	+0.27	3/2
Na I	+0.01	4/2	+0.04	4/3	+0.04	4/3	+0.14	4/2	+0.02	4/2
Mg I	−	−	+0.21	1/1	+0.04	1/2	+0.08	1/1	+0.18	2/2
Al I	−0.01	2/2	−0.01	2/2	−0.30	2/2	−0.29	1/2	−0.24	3/2
Si I	+0.03(7)	29/5	−0.06(19)	29/25	−0.22(19)	25/16	−0.12(14)	22/16	−0.12(13)	33/20
Si II	−	−	−0.25	3/2	−0.14	3/2	−0.15	2/2	−0.11	3/2
S I	−	−	+0.04	1/4	−0.07	1/4	+0.08	1/3	−0.01	1/5
Ca I	+0.03	11/4	+0.05(12)	11/8	−0.15(15)	8/8	−0.00(14)	11/7	−0.07(18)	12/9
Sc II	+0.06(5)	7/5	−0.10(13)	7/12	−0.18(13)	5/12	+0.02(20)	7/10	−0.06(17)	7/14
Ti I	+0.00(13)	37/9	+0.04(14)	37/55	−0.06(15)	26/42	+0.10(13)	12/29	+0.03(13)	45/81
Ti II	+0.01	11/1	−0.06(17)	11/24	−0.13(20)	8/24	+0.04(9)	7/16	−0.02(9)	14/28
V I	−0.03(14)	8/7	+0.08(15)	8/18	−0.06(11)	6/14	+0.07	4/7	+0.01(11)	10/27
Cr I	+0.00(9)	20/12	+0.01(10)	20/43	−0.15(17)	15/44	+0.02(16)	15/21	−0.03(15)	22/68
Cr II	−0.03(14)	7/6	−0.17(16)	7/9	−0.26(18)	7/14	−0.10(12)	5/9	−0.07(7)	7/15
Mn I	−0.12	7/4	−0.16(16)	7/20	−0.29	4/22	−0.20	4/14	−0.16(19)	7/26
Fe I	+0.03(7)	206/57	−0.08(17)	206/213	−0.19(18)	178/244	−0.09(16)	147/162	−0.09(15)	209/335
Fe II	+0.05(8)	23/6	−0.04(16)	23/78	−0.08(14)	21/35	+0.02(14)	17/26	−0.02(11)	26/41
Co I	−0.15(5)	8/5	−0.11(16)	8/35	−0.14(29)	7/26	+0.18	3/12	−0.01(17)	12/47
Ni I	−0.01(9)	61/31	−0.08(12)	61/85	−0.15(14)	45/78	−0.03(14)	34/44	−0.05(11)	67/97
Cu I	−0.08	2/1	−0.14	2/3	−0.33	2/3	+0.10	2/2	+0.09	3/2
Zn I	−	−	−0.08	2/3	−0.22	2/3	−0.20	2/3	−0.10	2/3
Y II	+0.05	5/2	−0.13(17)	5/11	−0.15(18)	6/12	+0.02(20)	6/8	−0.13(18)	6/14
Ba II	−	−	+0.01	1/3	−0.33	1/2	−0.19	1/1	−0.21	3/2

cf. the Boltzmann equation). By requiring that there must be no correlation with E_{low} and the least possible difference between neutral and ionized lines of the same element (from this point we call this "ion-balance") we have constrained T_{eff} and $\log g$. In the next Sections we will discuss the results for the stars with slow ($v \sin i < 25$ km s^{-1}) and moderate rotation.

5.1. Constraining T_{eff} and $\log g$ for the slow rotators

To give an impression of how well we can constrain the fundamental atmospheric parameters and the uncertainty of the derived abundances, we show the abundances found for different models for the stars HD 43318 in Fig. 5 and HD 57006 in Fig. 6. As discussed in Sec. 4.2.2 the abundance of each line is measured relative to the abundance found from the spectrum of the Sun where the zero points are from Grevesse & Sauval (1998). Open symbols indicate that less than five lines are used for the abundance estimate. Triangles are used to indicate a significant ($>1\sigma$) slope when fitting a line to abundance vs. E_{low}. The triangle symbol points down (up) if the correlation is negative (positive).

We will discuss in detail the results for HD 43318 shown in Fig. 5 for five different models. The parameters of the reference model is given below the plot ($T_{eff} = 6191$ K, $\log g = 4.0$, and microturbulence $\xi_t = 1.4$ km s^{-1}) and the adjustments for the different models are given as ΔT_{eff}, $\Delta \log g$, and $\Delta \xi_t$. For example, in model 2, we have added 209 K to T_{eff}. This essentially creates ion-balance for Fe and Cr but not for Ti. But a higher T_{eff} results in a negative correlation for Fe I abundance and E_{low} which is marked by a triangle symbol pointing down in Fig. 5. For model 3 we have decreased $\log g$ which also restores the ion-balance, but now a positive correlation of Fe II and E_{low} is the result. The model with $\Delta T_{eff} = 70$ K and $\Delta \log g = -0.3$ dex is our preferred model.

The results of four models of HD 57006 are compared in Fig. 6. These models have a much better agreement in the ion balance for both Si, Ti, Cr, and Fe. It is seen that changing $\log g$ by 0.2 dex or T_{eff} by 150 K in the model clearly breaks the ion balance and also results in correlations with Fe I abundance and E_{low}.

For the remaining slowly rotating stars we show the abundance pattern for the best models in the column 1–5 in Fig. 7.
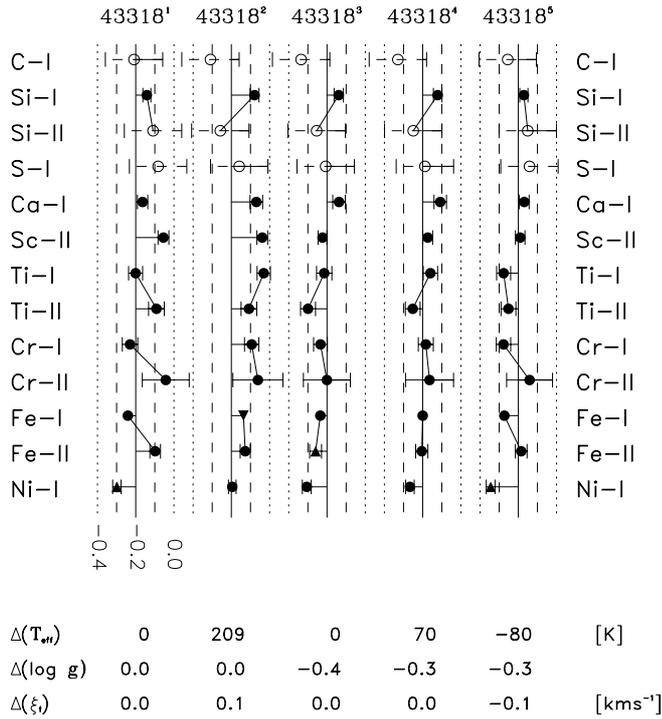
Fig. 5. Abundances for selected elements for five different models of HD 43318. Open symbols are used when less than five lines were used. Circle symbols are used when no significant correlation of abundance and lower excitation potential is found. The triangle symbol pointing down (up) are used when a significant negative (positive) correlation is found (see e.g. Fe I in model 2). The atmospheric parameters of the reference model is given below each panel and the relative parameters (*model – reference*) is given below the abundances.

It can be seen that the ion balance for Fe, Cr, and Fe is within the errors bars in all cases for these stars.

5.2. Constraining T_{eff} and $\log g$ for moderate rotators

Columns 6–9 in Fig. 7 shows the abundance pattern for the four stars with moderate $v \sin i$.

The star HD 49434 is a moderately fast rotator ($v \sin i = 84$ km s^{-1}). Here we find no usable Cr lines and thus have only used the ion balance for Fe to adjust T_{eff} and $\log g$, but with the constraint that there must be no correlation of Fe I abundance and E_{low}. This approach, however, is connected with large uncertainties due to the blending of lines. HD 49434 was also analysed by Bruntt et al. (2002). In the present study we have included more Fe I lines but our result agrees well with Bruntt et al. (2002).

The star HD 55057 has $v \sin i = 120$ km s^{-1} and there are only very few lines usable for abundance analysis.

For the moderately high rotators HD 171834 and HD 184663 ($v \sin i \simeq 50$–60 km s^{-1}) there is a highly significant difference in the abundance found from neutral and ionized lines of Cr and Fe. Adjusting $\log g$ and T_{eff} cannot produce a coherent result. The $\log g$ we have found for HD 171834 is 0.5 dex higher than what we find from the HIPPARCOS parallax and also results from the literature (cf. Table 4), but it is still within the large error of 0.5 dex.
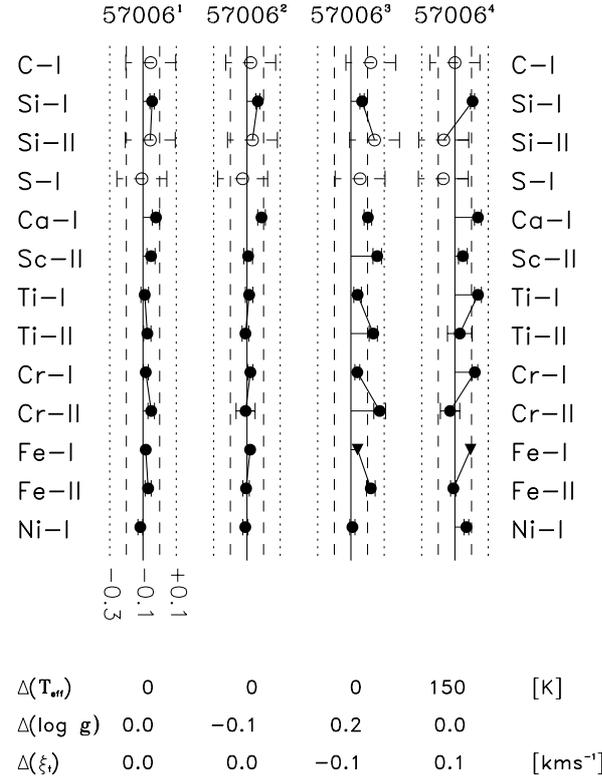
Fig. 6. Abundances for selected elements for four different models for HD 57006. See caption of Fig. 5 for details.

5.3. Summary of the parameter estimation

In Sect. 5.1 we have estimated how well we can constrain T_{eff} and $\log g$ for two slow rotators. From a similar analysis for all five slow rotators ($v \sin i < 15$ km s^{-1}) we find that we can constrain T_{eff} and $\log g$ to within 70–100 K and 0.1–0.2 dex, respectively. However, these error estimates do not include possible systematic errors due to the simplifications of the applied 1-D LTE atmospheric models. We are planning a future study of the importance of the applied models.

We have four stars in our sample with moderately high $v \sin i$ which makes it difficult to constrain the atmospheric parameters. The errors on T_{eff}, $\log g$, and [Fe/H] are about 200 K, 0.5 dex, and 0.15 dex, respectively.

With the analyses provided here $\log g$ cannot be constrained better than with the parallax from HIPPARCOS but it gives us an independent estimate. On the other hand we determine T_{eff} more accurately than from Strömgren photometry but not better than the temperatures from the line depth ratios. From the many iron lines the metallicity we find is determined to within 0.1 dex for the slow rotators ($v \sin i < 15$ km s^{-1}) and 0.2 dex for the faster rotators. In the former case this is a factor of two better than the metallicity determined from Strömgren photometry.

Our final T_{eff} and $\log g$ estimates are given in Table 4 under Ref. 1a along with the [Fe/H] found from the abundance analysis (cf. Sect. 6).
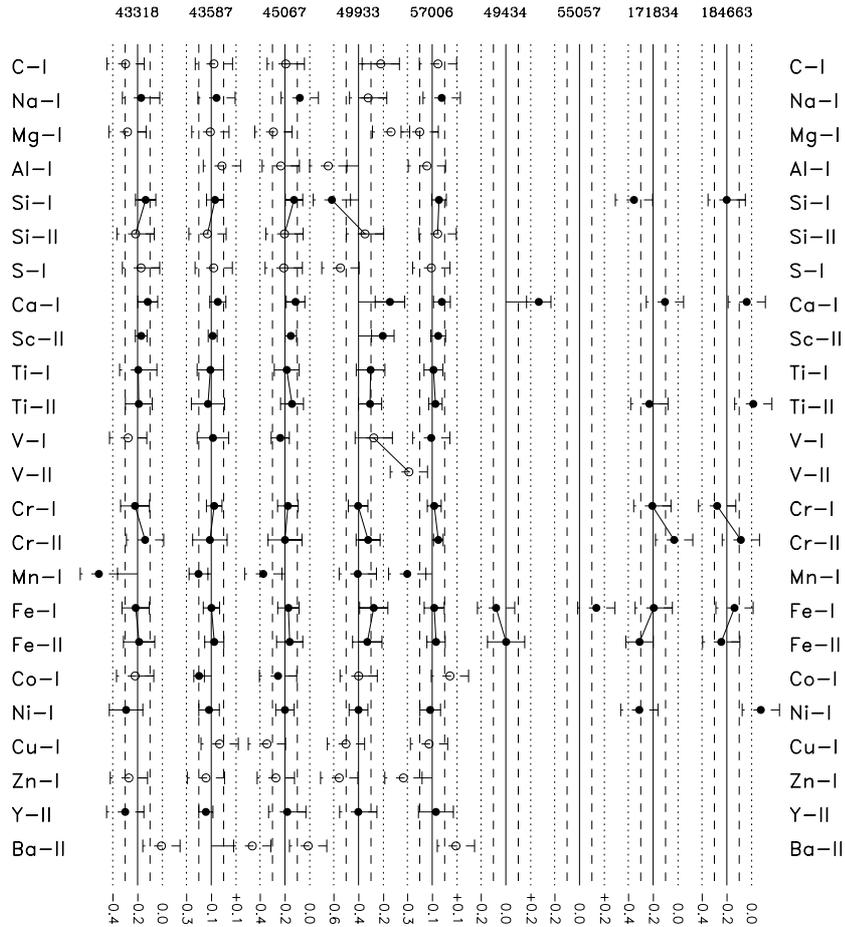
Fig. 7. Results of the abundance analysis of the proposed COROT main targets. For each star we plot the derived abundance relative to the Sun (Grevesse & Sauval 1998). The open symbols indicate that three or less lines were used. The error bars correspond to the rms errors but only if the error is smaller than 0.15 dex and more than five lines were used. Otherwise a dashed error bar corresponding to 0.15 dex is plotted. Elements of the same species are connected with a solid line. The results shown here are also given in Table 7).

6. Abundances of the COROT targets

In Sect. 4 three different methods to compute abundances were applied to a subset of our sample, and we obtained similar results within the error bars. For the analysis of the whole sample method A (VWA semi-automatic software) has been adopted and the results are given here.

Abundances relative to the Sun for nine potential COROT targets is shown in Fig. 7. The first five stars plotted (HD 43318 to HD 57006) are the slow rotators for which the best results are obtained. From the abundance patterns we find no evidence of classical chemically peculiar stars.

For the slowly rotating stars, the lines of Mn give a systematically lower abundance, indicating a systematic error. We have found that for this specific element, the hyperfine structure levels are not always found in VALD, thus yielding an erroneous result. We also find a relative over-abundance of Ba, but we only have few lines for this element.

The abundances are also given in Table 7. The parameters of the atmospheric models used are given in Table 4 under Ref. 1a. The abundances are given relative to the solar abundances found by Grevesse & Sauval (1998) which are found in the first column in Table 7. In the parentheses we

give the rms standard deviation based on the line-to-line scatter, but only if at least four lines were used. As an example we find for Ca I in HD 43318 the result −0.12(8) which means $\log N_{Ca}/N_{tot} - (\log N_{Ca}/N_{tot})_\odot = -0.12 \pm 0.08$. We give the rms error from 8 lines, and the standard deviation of the mean is 0.03 dex. The number of lines used to determine the abundance is in the column with label n.

In addition to the quoted errors contributions from the abundance zero points (Grevesse & Sauval 1998) of the order 0.05 dex and model dependent uncertainties of the order 0.05–0.10 (0.20) dex for the slow (fast) rotators must be added. Thus, we can constrain the metallicity [Fe/H] to about 0.10 (0.20) dex. In Table 4 we have given [Fe/H] as the mean of the iron abundance relative to the Sun found from Fe I and Fe II lines for all three methods described in Sect. 4.

7. Conclusions and future prospects

– We have performed a detailed abundance analysis of nine potential COROT main targets. The accuracy of the abundances of the main elements is of the order 0.10 dex when including possible errors on microturbulence and inadequacies of the applied 1D LTE atmospheric models.

Table 7. Results of the abundance analysis of corot targets using vwa (method A). For all stars except HD 49933, HD 49434, HD 55057, HD 171834, and HD 184663 the abundances are measured relative to the Sun, i.e. the mean of the line-by-line differences. For the other stars the abundances are given relative to the standard solar abundances given in first column (Grevesse & Sauval 1998). The rms errors are found in the parentheses and the number of lines used, n, is given. For example, the result "−0.12(8) 8" for Ca in HD 43318 means $\log N_{Ca}/N_{tot} - (\log N_{Ca}/N_{tot})_\odot = -0.12 \pm 0.08$ as found from eight lines.

| | | HD 43318 | | HD 43587 | | HD 45067 | | HD 49933 | | HD 57006 | |
$\log(N/N_{tot})_\odot$	Element	ΔA	n	ΔA	n	ΔA	n	ΔA	n	ΔA	n
−3.49	C I	−0.30	2	−0.08(8)	3	−0.19(16)	3	−0.22	2	−0.05(9)	3
−5.71	Na I	−0.17(17)	4	−0.06(4)	4	−0.08(12)	4	−0.32	1	−0.02(13)	4
−4.46	Mg I	−0.28	2	−0.11	1	−0.29	1	−0.14	2	−0.20	1
−5.57	Al I	−	−	−0.01	2	−0.23	2	−0.64	1	−0.14	1
−4.49	Si I	−0.14(8)	15	−0.07(6)	29	−0.13(7)	25	−0.61(36)	20	−0.05(5)	22
−4.49	Si II	−0.22	2	−0.13(9)	3	−0.20	3	−0.35(8)	3	−0.06	2
−4.71	S I	−0.17	1	−0.08	1	−0.21	1	−0.55	1	−0.11	1
−5.68	Ca I	−0.12(8)	8	−0.05(6)	11	−0.11(7)	8	−0.15(11)	18	−0.02(6)	11
−8.87	Sc II	−0.17(4)	5	−0.09(3)	7	−0.15(4)	5	−0.20(9)	7	−0.05(5)	7
−7.02	Ti I	−0.19(16)	19	−0.11(10)	37	−0.19(10)	26	−0.30(11)	26	−0.09(7)	12
−7.02	Ti II	−0.19(10)	10	−0.13(13)	11	−0.14(9)	8	−0.31(9)	23	−0.07(5)	7
−8.04	V I	−0.28	3	−0.09(12)	8	−0.24(7)	6	−0.28	1	−0.11(12)	4
−8.04	V II	−	−	−	−	−	−	+0.00	1	−	−
−6.37	Cr I	−0.22(11)	12	−0.08(6)	20	−0.18(8)	15	−0.40(7)	20	−0.08(5)	15
−6.37	Cr II	−0.14(26)	5	−0.11(13)	7	−0.20(13)	7	−0.32(9)	19	−0.05(3)	5
−6.65	Mn I	−0.51(14)	4	−0.20(7)	7	−0.37(9)	4	−0.41(17)	10	−0.30(2)	4
−4.54	Fe I	−0.22(10)	141	−0.10(6)	206	−0.17(8)	178	−0.28(11)	218	−0.08(8)	147
−4.54	Fe II	−0.19(12)	18	−0.08(7)	23	−0.16(10)	21	−0.33(11)	34	−0.07(7)	17
−7.12	Co I	−0.22(25)	3	−0.20(4)	8	−0.26(22)	7	−0.40	2	+0.04(16)	3
−5.79	Ni I	−0.29(13)	36	−0.12(8)	61	−0.20(7)	45	−0.40(7)	35	−0.12(8)	34
−7.83	Cu I	−	−	−0.03	2	−0.34	2	−0.50	1	−0.13	2
−7.44	Zn I	−0.27	2	−0.14	2	−0.27	2	−0.56(6)	3	−0.33	2
−9.80	Y II	−0.30(18)	4	−0.14(5)	5	−0.18(16)	6	−0.40(8)	4	−0.07(14)	6
−9.91	Ba II	−0.01	1	+0.23	1	−0.01	1	+0.48(23)	3	+0.09	1

| | | HD 49434 | | HD 55057 | | HD 171834 | | HD 184663 | |
$\log(N/N_{tot})_\odot$	Element	ΔA	n	ΔA	n	ΔA	n	ΔA	n
−4.49	Si I	−	−	−	−	−0.35(68)	9	−0.20(60)	10
−5.68	Ca I	+0.26(9)	8	−	−	−0.11(40)	10	−0.04(23)	9
−7.02	Ti II	−	−	−	−	−0.23(24)	13	+0.01(29)	9
−6.37	Cr I	−	−	−	−	−0.21(60)	6	−0.28(28)	7
−6.37	Cr II	−	−	−	−	−0.03(24)	9	−0.09(40)	6
−4.54	Fe I	−0.08(22)	37	+0.14(29)	19	−0.20(30)	60	−0.14(31)	102
−4.54	Fe II	+0.00(14)	7	−	−	−0.31(11)	7	−0.24(27)	9
−5.79	Ni I	−	−	−	−	−0.31(43)	18	+0.07(40)	12

– We have compared three different methods for the analysis which show very good agreement. The discrepancies are due to the different parameters we have used for the stellar atmosphere models.

– We have found no evidence for chemically peculiar stars.

– We have constrained T_{eff}, $\log g$, and metallicity to within 70−100 K, 0.1−0.2 dex, and 0.1 dex for the five slow rotators in our sample. For the four moderate rotators we cannot constrain the fundamental parameters very well, i.e. T_{eff}, $\log g$, and [Fe/H] to within 200 K, 0.5 dex, and 0.15 dex.

– For most of the stars our results for the fundamental parameters agree with the initial estimates from Strömgren photometry, line depth ratios, and Hα lines, and the hipparcos parallaxes. For HD 43318 we have found a somewhat lower T_{eff} and $\log g$. For HD 49933 we find a T_{eff} about 200 K hotter than previous studies. For the fast

rotators HD 171834 and HD 184663 we find a quite high $\log g$ value compared to other methods, but the uncertainty on our estimate is large (0.5 dex).

– For the two corot targets HD 46304 and HD 174866 abundance analyses were not possible due to the very high $v \sin i$.

Suggestions for future studies of the corot targets:

– From the comparison of two independent analyses (method A and C; cf. 4.5) we have found evidence that a careful (re-)normalization of the spectra may be very important but this must be investigated further.

– To probe the interior of the stars with the asteroseismic data from corot we need to know the abundances of elements which affect the evolution of the stars, namely C, N, and O. Thus, spectra that cover the infrared regions with good C, N, and O lines must be obtained.

– Recent 3D atmospheric models should also be used in the analysis to explore the importance of the models.

We finally note that the next paper in this series will give the results of the abundance analysis for some recently proposed COROT primary targets, the possible secondary COROT targets, as well as the proposed targets for the MONS/RØMER mission.

References

Anstee, S. D., & O'Mara, B. J. 1995, MNRAS, 276, 859
Anstee, S. D., O'Mara, B. J., & Ross, J. E. 1997, MNRAS, 284, 202
Axer, M., Fuhrmann, K., & Gehren, T. 1994, A&A, 291, 895
Baglin, A., Auvergne, M., Catala, C., Michel, E., & COROT Team 2000, Proc. of the SOHO 10/GONG 2000 Workshop ed. A. Wilson, & P. L. Pallé, 2001, ESA SP-464, 395
Balachandran, S. 1990, ApJ, 354, 310
Baranne, A., Queloz, D., Mayor, M., et al. 1996, A&AS, 119, 373
Barklem, P. S., & O'Mara, B. J. 2000, MNRAS, 311, 535
Bessell, M. S., Castelli, F., & Plez, B. 1998, A&A, 333, 231
Bikmaev, I. F., Ryabchikova, T. A., Bruntt, H., et al. 2002, A&A, 389, 537
Bruntt, H., Catala, C., Garrido, R., et al. 2002, A&A, 389, 345
Delbouille, L., Roland, G., & Neven, L. 1973, Atlas photometrique du spectre solaire, Universite de Liege, Institut d'Astrophysique
Canuto, V. M., & Mazzitelli, I. 1991, ApJ, 370, 295
Canuto, V. M., & Mazzitelli, I. 1992, ApJ, 389, 724
Cayrel, R., Cayrel de Strobel, G., & Campbell, B. 1985, A&A, 146, 249
Cayrel de Strobel, G., Cayrel, R., Friel, E., Zahn, J. P., & Bentolila, C. 1994, A&A, 291, 505
Cayrel de Strobel, G., Soubiran, C., & Ralite, N. 2001, A&A, 373, 159
Donati, J. F., Semel, M., Carter, B. D., Rees, D. E., & Cameron, A. C. 1997, MNRAS, 291, 658
Edvardsson, B., Andersen, J., Gustafsson, B., et al. 1993, A&A, 275, 101
ESA 1997, The Hipparcos and Tycho Catalogues, ESA SP-1200
Favata, F., Micela, G., & Sciortino, S. 1997, A&A, 323, 809,
Fuhrmann, K., Axer, M., & Gehren, T. 1993, A&A, 271, 451
Galazutdinov, G. 1992, SAO RAS Preprint No. 92
Girardi, L., Bressan, A., Bertelli, G., & Chiosi, C. 2000, A&AS, 141, 371
Gratton, R. G., Carretta, E., & Castelli, F. 1996, A&A, 314, 191
Grevesse, N., & Sauval, A. J. 1998, Space Sci. Rev., 85, 161
Hartmann, K., & Gehren, T. 1988, A&A, 199, 269
Hauck, B., & Mermilliod, M. 1998, A&AS, 129, 431
Heiter, U., Kupka, F., van't Veer-Menneret, C., et al. 2002, A&A, 392, 619
Kovtyukh, V. V., Soubiran, C., Belik, S. I., & Gorlova, N. I. 2003, A&A, 411, 559
Kupka, F. 1996, ASP Conf. Ser., 108, ed. S. J. Adelman, F. Kupka, & W. W. Weiss, 73
Kupka, F., & Bruntt, H. 2001, First COROT/MONS/MOST Ground-based Support Workshop, p. 39, ed. C. Sterken, University of Brussels
Kupka, F., Piskunov, N., Ryabchikova, T. A., Stempels, H. C., & Weiss, W. W. 1999, A&AS, 138, 119
Kurucz, R. L. 1993, CD-ROM 18, ATLAS9 Stellar Atmosphere Programs and 2 km/s Grid
Kurucz, R. L. 1998, http://cfaku5.harvard.edu/
Lastennet, E., Lignières, F., Buser, R., et al. 2001, A&A, 365, 535
Perrin, M. N. 1976, Ph.D. Thesis
Rogers, N. Y. 1995, Comm. Asteroseismol., 78
Smalley, B., & Kupka, F. 1997, A&A, 328, 349
Valenti, J. A., & Piskunov, N. 1996, A&AS, 118, 595
Vidal, C. R., Cooper, J., & Smith, E. W. 1973, ApJS, 25, 37
Vogt, S. S., Butler, R. P., Marcy, G. W., et al. 2002, ApJ, 568, 352
Zakhozhaj, V. A., & Shaparenko, E. F. 1996, Kinematika i Fizika Nebesnykh Tel, 12, 20